Cholesterol-tethered platinum II-based supramolecular nanoparticle increases antitumor efficacy and reduces nephrotoxicity

Poulomi Sengupta[a,b,1], Sudipta Basu[a,b,1,2,3], Shivani Soni[a,b,1,4], Ambarish Pandey[a,b,5], Bhaskar Roy[a,b,5], Michael S. Oh[a,b], Kenneth T. Chin[c], Abhimanyu S. Paraskar[a,b], Sasmit Sarangi[a,b], Yamicia Connor[a,b,d], Venkata S. Sabbisetti[b,e], Jawahar Kopparam[a,b], Ashish Kulkarni[a,b], Katherine Muto[c], Chitra Amarasiriwardena[f,g], Innocent Jayawardene[f,g], Nicola Lupoli[f,g], Daniela M. Dinulescu[b,c], Joseph V. Bonventre[b,e], Raghunath A. Mashelkar[a,h], and Shiladitya Sengupta[a,b,d,i,j,3]

[a]Laboratory for Nanomedicine, Division of Biomedical Engineering, Department of Medicine and Center for Regenerative Therapeutics, [e]Renal Division and Division of Biomedical Engineering, [c]Department of Pathology, and [g]Channing Laboratory, Brigham and Women's Hospital, Cambridge, MA 02139; [b]Harvard Medical School, Boston, MA 02115; [d]Harvard–MIT Division of Health Sciences and Technology, Cambridge, MA 02139; [f]Harvard School of Public Health, Boston, MA 02215; [h]National Chemical Laboratories, Pune 411021, India; [i]Indo–United States Joint Center for Nanobiotechnology, Cambridge, MA 02139; and [j]Dana-Farber Cancer Institute, Brookline, MA 02445

Edited* by Jean-Marie P. Lehn, Universite de Strasbourg, Strasbourg Cedex, France, and approved May 28, 2012 (received for review February 22, 2012)

Nanoscale drug delivery vehicles have been harnessed extensively as carriers for cancer chemotherapeutics. However, traditional pharmaceutical approaches for nanoformulation have been a challenge with molecules that exhibit incompatible physicochemical properties, such as platinum-based chemotherapeutics. Here we propose a paradigm based on rational design of active molecules that facilitate supramolecular assembly in the nanoscale dimension. Using cisplatin as a template, we describe the synthesis of a unique platinum (II) tethered to a cholesterol backbone via a unique monocarboxylato and O→Pt coordination environment that facilitates nanoparticle assembly with a fixed ratio of phosphatidylcholine and 1,2-distearoyl-*sn*-glycero-3-phosphoethanolamine-*N*-[amino (polyethylene glycol)-2000]. The nanoparticles formed exhibit lower IC_{50} values compared with carboplatin or cisplatin in vitro, and are active in cisplatin-resistant conditions. Additionally, the nanoparticles exhibit significantly enhanced in vivo antitumor efficacy in murine 4T1 breast cancer and in K-Ras$^{LSL/+}$/Pten$^{fl/fl}$ ovarian cancer models with decreased systemic- and nephro-toxicity. Our results indicate that integrating rational drug design and supramolecular nanochemistry can emerge as a powerful strategy for drug development. Furthermore, given that platinum-based chemotherapeutics form the frontline therapy for a broad range of cancers, the increased efficacy and toxicity profile indicate the constructed nanostructure could translate into a next-generation platinum-based agent in the clinics.

chemotherapy | nanomedicine

Cancer remains one of the main causes of death in the United States and many western countries. In addition, the incidence is also increasing in less developed and economically transitioning countries (1). The World Health Organization projects over 12 million deaths worldwide in 2030 because of cancer, up from 7.6 million in 2008 (2). To address this growing problem, there is an urgent need to develop treatment strategies that are more efficaceous with lesser adverse effects. An increasingly pursued approach to achieve these goals is the use of nanotechnology to preferentially target anticancer agents to solid tumors (3). This approach capitalizes on the unique leaky angiogenic tumor vasculature coupled with impaired intratumoral lymphatic drainage, contributing to an enhanced permeation and retention (EPR) effect (4). Indeed, nanoparticles carrying a doxorubicin payload or an albumin-paclitaxel nanocomplex increase intratumoral drug concentration (5, 6) and are currently in the clinics (7). However, traditional processes for nanoformulation are often incompatible with physicochemical properties of many chemotherapeutic agents, which limit the entrapment efficiency or introduce suboptimal release kinetics. To address these challenges, we propose a unique paradigm moving beyond traditional encapsulation strategies to the rational design of molecules that facilitate supramolecular assembly in the nanoscale dimension. In this study, we decided to use cisplatin [*cis*-dichlorodiamineplatinum (II)] as an example to test this hypothesis. Cisplatin is one of the most widely used chemotherapeutic agents (8) but poses significant challenges for nanoformulations (9, 10). For example, SPI-077, a sterically stabilized liposome encapsulating cisplatin, exhibited poor clinical efficacy resulting from impaired drug release (11, 12).

To achieve supramolecular nanoassembly, we synthesized a cholesterol-tethered cisplatinum (II) amphiphile. The design of the tether was inspired by the process of "aquation," wherein the chloride leaving groups of cisplatin are rapidly displaced to form *cis*-Pt$[(NH_3)_2(OH_2)Cl]^+$ and *cis*-Pt$[(NH_3)_2(OH_2)_2]^{2+}$ (8). Self-assembling cholesterol-succinic acid-cisplatinum II-based nanoparticles (SACNs) exhibited increased potency and efficacy in vitro and in vivo, respectively. Additionally, the SACNs exceed the size cutoff for clearance by the kidney (13), and therefore exhibited limited cisplatin-associated nephrotoxicity (14). We demonstrate that rational drug design can enable the increase in the supramolecular dimension from the Angstrom- to the nano-scale, thereby conferring unique biological properties. Furthermore, only three platinates—cisplatin, carboplatin, and oxaliplatin—have been successfully used in the clinics (8). The increased efficacy with improved therapeutic index of the current molecule compared with the existing platinates indicates the

Author contributions: P.S., S.B., S. Soni, A.P., B.R., A.S.P., V.S.S., A.K., D.M.D., R.A.M., and S. Sengupta designed research; P.S., S.B., S. Soni, A.P., B.R., M.S.O., K.T.C., A.S.P., S. Sarangi, Y.C., V.S.S., J.K., A.K., K.M., C.A., I.J., N.L., and D.M.D. performed research; P.S., S.B., S. Soni, A.P., B.R., M.S.O., K.T.C., A.S.P., S. Sarangi, Y.C., V.S.S., D.M.D., J.V.B., and S. Sengupta analyzed data; and P.S., S.B., S. Soni, A.P., B.R., V.S.S., D.M.D., R.A.M., and S. Sengupta wrote the paper.

Conflict of interest statement: P.S., S.B., S. Soni, A.S.P., and S. Sengupta are listed as inventors on a patent filed by Brigham and Women's Hospital.

*This Direct Submission article had a prearranged editor.

Freely available online through the PNAS open access option.

[1]P.S., S.B., and S. Soni contributed equally to this work.

[2]Present address: Department of Chemistry, Indian Institute of Science Education and Research (IISER) Pune, Sutarwadi, Pashan, Pune, Maharashtra, 411021, India.

[3]To whom correspondence may be addressed. E-mail: ssengupta2@partners.org, or sudipta.basu@iiserpune.ac.in.

[4]Present address: Department of Biological Sciences, Alabama State University, Montgomery, AL 36104.

[5]A.P. and B.R. contributed equally to this work.

This article contains supporting information online at www.pnas.org/lookup/suppl/doi:10.1073/pnas.1203129109/-/DCSupplemental.

potential for clinical translation as the next-generation platinum-based chemotherapeutic.

Results

Synthesis of Cholesterol-Succinic Acid-Pt(II) Molecule. Aquation of cisplatin results in the rapid formation of active species *cis*-$[Pt(NH_3)_2Cl(OH_2)]^+$ and *cis*-$[Pt(NH_3)_2(OH_2)_2]^{2+}$ with a rate constant of 8×10^{-5} s^{-1} (15). In contrast, the rate constant for aquation of carboplatin, where the platinum is coordinated with a stable bidentate 1,1-cyclobutanedicarboxylato ligand, was found to be 7.2×10^{-7} s^{-1}. This difference in their rate of aquation was matched by their rates of binding to DNA, indicating that the rate of aquation correlates with potency (16, 17). Indeed, we had demonstrated that Pt chelated to a polyisobutylene maleic acid glucosamine copolymer via a monocarboxylato and an O→Pt coordinate bond release of Pt in a pH-dependent manner, and more efficiently than when the Pt was chelated using dicarboxylato bonds or via a monocarboxylato and an N→Pt coordinate bond (18, 19). As a result, we rationalized that the introduction of a coordination environment where the Pt was chelated via a monocarboxylato and an O→Pt coordinate bond is critical to the design of an efficacious platinate. As outlined in the given scheme (Fig. 1*A*), we first synthesized cholesterol-ethylenediamine conjugate in near quantitative yield (99.1%) by reacting cholesteryl chloroformate with excess ethylene diamine. Next, we introduced monocarboxylato and amide chelating moiety by reacting cholesterol-ethylenediamine conjugate with succinic anhydride (at 95% yield). Finally, the conjugate was reacted with aquated *cis*-$Pt[(NH_3)_2(OH_2)_2]^{2+}$ in 1:1 molar ratio in acidic pH (pH = 6.4) to obtain cholesterol-cisplatin conjugate, characterized by monocarboxylato and an O→Pt coordinate bond of an amide, as indicated by an unique single ^{195}Pt NMR peak at −1,621.497 ppm (Fig. S1). All of the other intermediates were characterized by ^1H and ^{13}C NMR spectroscopy (Figs. S2–S5).

Synthesis and Characterization of SACNs. We engineered the SACNs from the cholesterol-succinic acid-platinum (II) molecule, phosphatidylcholine (PC) and 1,2-distearoyl-*sn*-glycero-3-phosphoethanolamine-*N*-[amino(polyethylene glycol)-2000] (DSPE-PEG) in 1:2:0.2 weight ratio using a lipid-film hydration self assembly method (20) (Fig. 1*A*). The ultrastructure analysis using cryo-transmission electron microscopy (cryo-TEM) (Fig. 1*B*) revealed the formation of predominantly uni- and rare multilamellar structures less than 200 nm in diameter, with a membrane thickness ∼5 nm. Dynamic light scattering further confirmed the size distribution of SACNs with a mean hydrodynamic diameter of 141.4 ± 1.2 nm (n = 9) (Fig. 1*C*). To validate the kinetics of cisplatin release, SACNs were incubated at acidic pH 5.5 over 120 h, with pH 7 as a reference. As shown in Fig. 1*D*, SACNs exhibited a pH-dependent sustained release of cisplatin. Interestingly, the rate of release was slower than observed earlier using a polymeric system, indicating that the cholesterol can incorporate into the lipid layer in a manner where the Pt moiety is present both on the outer as well as inner part of the membrane.

In Vitro Efficacy of SACNs. To evaluate the efficacy of the SACNs in vitro, we performed a cell viability assay using Lewis lung carcinoma (LLC) and 4T1 breast cancer cell lines. Cell viability was quantified by using a 3-(4,5-dimethylthiazol-2-yl)-5-(3-carboxymethoxyphenyl)-2-(4-sulfophenyl)-2H-tetrazolium, inner salt assay at 48 h postincubation. As shown in Fig. 2 *A* and *B*, free cisplatin induced LLC and 4T1 cell kill with IC_{50} values of 2.91 ± 0.015 μM and 4.72 ± 0.016 μM, respectively. In neither of these cell lines did carboplatin exert any inhibitory activity at this concentration range. Interestingly, the SACNs were found to be more efficacious than cisplatin against both 4T1 and LLC cells, with IC_{50} values of 0.44 ± 0.016 μM and 1.16 ± 0.016 μM, respectively. We next tested the efficacy of the SACNs in a cisplatin-resistant hepatocellular carcinoma (7404-CP20) cell line.

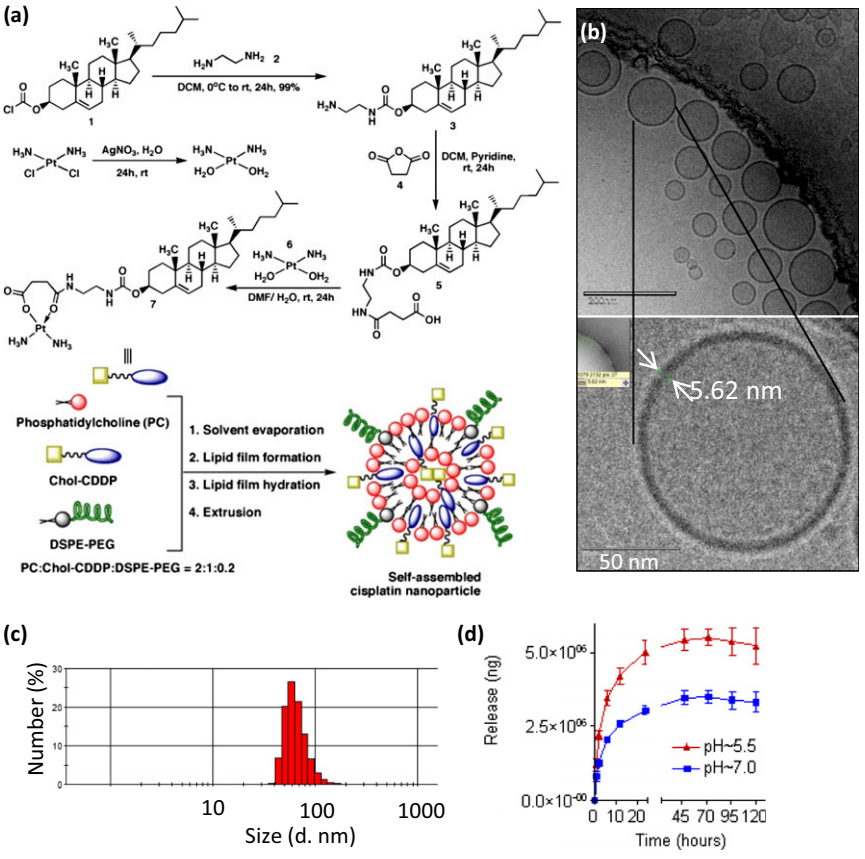

Fig. 1. Synthesis and characterization of SACNs. (*A*) Scheme for synthesis of cholesterol-cisplatin conjugate from cholesteryl chloroformate. Schematic representation shows synthesis of SACNs by self-assembly from PC, cholesterol-cisplatin conjugate, and DSPE-PEG. (*B*) High-resolution cryo-TEM image of SACNs at lower magnification (*Upper*) and magnified image (*Lower*). (Scale bar, *Upper*, 500 nm). (*C*) Distribution of hydrodynamic diameter of SACNs measured using dynamic light scattering. (*D*) Graph shows the pH-dependent release of platinum from SACNs as quantified over a 120-h period.

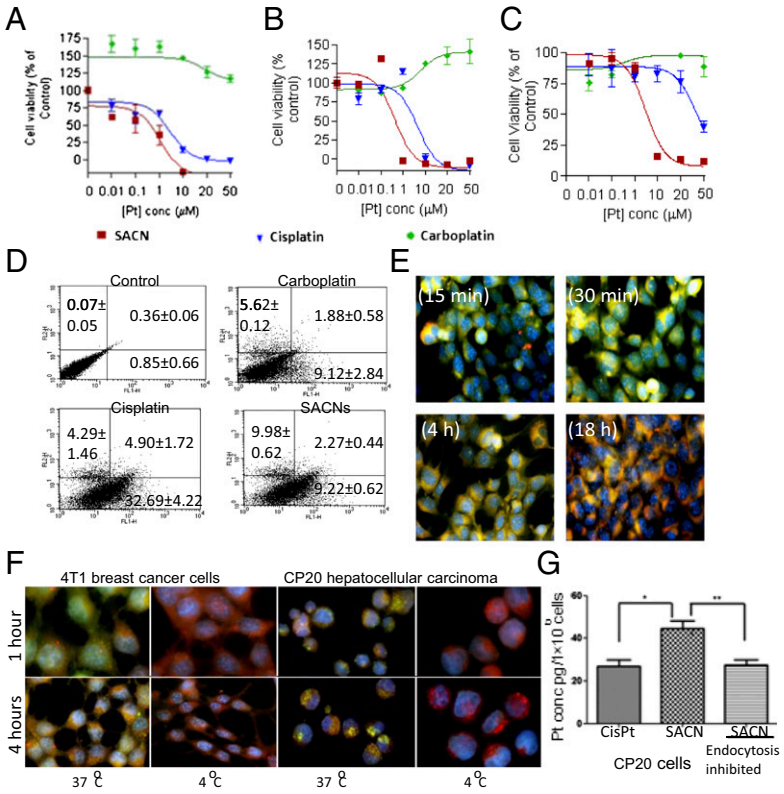

Fig. 2. In vitro characterization of SACNs. (*A*–*C*) Graphs show cell viability of (*A*) LLC, (*B*) 4T1, and (*C*) 7404-CP20 cell lines, respectively, after 48-h incubation with increasing concentrations of cisplatin, carboplatin, and SACNs. (*D*) Treatment with SACNs induces cell death by apoptosis. Representative FACS distribution of 4T1 cells treated with carboplatin, cisplatin, and SACNs at 1 μM Pt concentration. The cells were incubated for 24 h, following which they were labeled with Annexin-V FITC and counter-stained with propidium iodide. Each quadrant represents the percentage of cells in early apoptosis (*Lower Right*), late apoptosis (*Upper Right*), necrosis (*Upper Left*), and healthy cells (*Lower Left*). Data shown are mean ± SE from $n = 3$ independent experiments. (*E*) Representative epifluorescence imaging of 4T1 tumor cells for monitoring internalization of SACNs. SACNs were labeled with FITC (green), the endolysosomal compartment was labeled by LysoTracker red, and the nucleus was labeled with DAPI blue. Colocalization of the signals in the merged images reveals internalization of FITC-SACNs in the endolysosomal compartments within 4 h. (*F*). Epifluorescence imaging of 4T1 and CP20 tumor cells to monitor the internalization of FITC tagged SACN at 37 °C and 4 °C. Images were captured using a Nikon Ti epifluorescence microscope at 40× magnification. 4T1 images were captured at 1,000 × 700 pixel resolution and the 7404-CP20 images are 900 × 600 pixels. (*G*) Graph shows Pt levels in 7404-CP20 cells treated with cisplatin or SACNs (20 μM Pt concentration). Cells incubated with similar concentration of SACNs at 4 °C to inhibit energy-dependent endocytosis exhibit lower intracellular Pt concentrations (*$P < 0.05$, **$P < 0.01$, ANOVA, Newman–Keuls post hoc test).

Although the IC_{50} value for free cisplatin in this assay was calculated to be 42.84 ± 0.04 μM, consistent with previously reported values (21), the SACNs were found to be overcome the resistance with an IC_{50} value of 3.02 ± 0.013 μM (Fig. 2*C*). To elucidate the mechanism of cell death, we incubated 4T1 cells with a sub-IC_{50} concentration of the SACNs, cisplatin or carboplatin, for 24 h. The cells were labeled with FITC-Annexin V that binds to phosphatidylserine, an early marker for apoptosis. As seen in Fig. 2*D*, treatment with platinates induced both apoptosis and necrosis of the tumor cells, with both cisplatin and SACNs being more efficacious than carboplatin. Studies using FITC-labeled SACNs revealed that the nanoparticles were internalized and localized in the endolysosomal compartment in a temporal manner (Fig. 2*E*). This finding is further validated by incubating the tumor cells (4T1 and 7404-CP20) with FITC-labeled SACNs at 37 °C and 4 °C, wherein the internalization of SACNs into the cells was decreased in the latter condition (Fig.2*F*). To dissect the mechanism underlying the efficacy of SACNs in the cisplatin-resistant 7404-CP20 cell line, we quantified the intracellular concentration of Pt in the cells following incubation with cisplatin or SACNs containing equivalent levels of Pt. As shown in Fig. 2*G*, the SACNs resulted in significantly elevated intracellular levels of Pt compared with cisplatin. Incubating cells with SACNs at 4 °C, which inhibits energy-dependent endocytosis, reduced the intracellular Pt concentration to cisplatin-treated levels, validating that the SACNs can enter these cells via endocytosis.

Efficacy of SACNs in an in Vivo 4T1 Breast Cancer Model. Motivated by the sustained release of Pt and enhanced in vitro efficacy of SACNs, we evaluated its antitumor efficacy in vivo. As the first step, we established the maximum tolerated dose (MTD) for the SACNs in BALB/c mice to be 16 mg/kg compared with 9 mg/kg of cisplatin (Fig. 3*A*). We next dosed syngeneic BALB/c mice bearing 4T1 breast tumors (mean tumor volume ~100 mm^3) with a single dose of cisplatin (8 mg/kg). Other groups of animals received vehicle, carboplatin, or SACNs, (the latter two received a Pt dose equivalent to 8 mg/kg dose of cisplatin). As shown in Fig. 3*B*, although all of the platinates resulted in significant tumor inhibition compared with the vehicle-treatment, the SACNs exerted the maximal tumor inhibition ($P < 0.01$ vs. control) followed by cisplatin and carboplatin. Furthermore, although treatment with carboplatin or cisplatin exerted only minor increase in survival over vehicle-treated controls, the SACNs significantly increased overall survival trend (Fig. 3*C*). We next tested the effects of multiple low-dose treatment with cisplatin, carboplatin, or the SACNs, with the highest platinum dose in each case adding up to the levels of Pt delivered at the MTD of cisplatin. Two additional groups were included that were treated with a lower dose of cisplatin or SACNs (equivalent of 1 mg/kg dose of platinum). As shown in Fig. 3 *D* and *E*, treatment with cisplatin resulted in a dose-dependent inhibition of tumor growth. Interestingly, although at the highest doses the tumor inhibition with the SACNs or cisplatin were identical, at the lower doses the SACNs exerted a superior antitumor effect compared with free cisplatin ($P < 0.05$, ANOVA). Furthermore, cisplatin resulted in a significant reduction in mean body weight ($P < 0.05$, ANOVA) compared with the SACN-treated groups (Fig. 3*F*), indicating that the latter can reduce the systemic toxicity associated with cisplatin chemotherapy. Interestingly, even at the lower dose both the SACNs and cisplatin exerted greater tumor inhibition as opposed to the higher dose of carboplatin (Fig. 3 *E* and *F*). At the higher dose, both cisplatin and SACNs were found to increase survival, although the latter was superior (Fig. 3*G*). To elucidate the mechanism underlying of increased in vivo efficacy, the tumors were excised posttreatment and processed for TUNEL as a marker for apoptosis. As shown in Fig. 3*D*, SACNs induced significantly greater apoptosis than cisplatin, but at the higher doses both the SACNs and cisplatin induced similar apoptosis, consistent with the tumor inhibition results. However, at the latter dose level, cisplatin but not SACNs resulted in significant nephrotoxicity as evident by reduced kidney weight and up-regulation of kidney injury molecule-1 (KIM1) expression (Fig. 4 *A* and *B*). Additionally, TUNEL of the excised

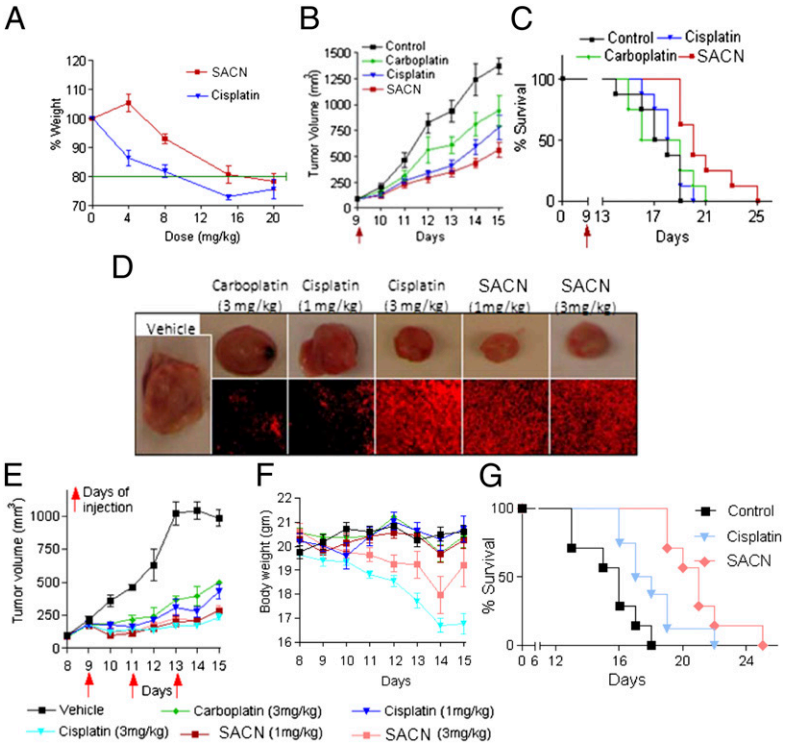

Fig. 3. In vivo antitumor activity of SACNs in 4T1 breast cancer model. (*A*) Graph shows body weight loss of animals with increasing doses of cisplatin or SACNs (Cisplatin NP). Maximum tolerated dose is calculated at 20% body weight loss. (*B*) Graph shows change in tumor volume in different treatment groups in 4T1 murine breast cancer model following a single dose of platinum chemotherapy at the MTD platinum dose of cisplatin. (*C*) Kaplan–Meier curve shows effect of different treatments on survival at MTD platinum dose of cisplatin ($P = 0.0189$ Logrank test for trend). (*D*) Multiple-dose effects of treatment on 4T1 breast cancer growth. Cells were implanted subcutaneously on day 0. Mice were treated with PBS, carboplatin (3 mg/kg), cisplatin (3 mg/kg and 1 mg/kg), and SACNs (3 mg/kg and 1 mg/kg) ($n = 4$, doses are Pt equivalent) on days 9, 11, and 13 posttumor implantation. *Upper* row shows representative images of excised tumors, and *Lower* row shows tumor cross sections processed for TUNEL as marker for apoptosis. Images were captured using a Nikon Ti epifluorescence microscope at 20× magnification to capture a large view field. (*E*) Growth curves show the effect of the different multiple-dose treatments on tumor volume. (*F*) Graph shows change in body weight of animals in different treatment groups. (*G*) Kaplan–Meier curve shows effect of different treatments on survival ($P = 0.0022$, Logrank Mantel–Cox test).

kidney sections (Fig. 4*C*) indicated significant apoptosis in cisplatin-treated mice, whereas the SACNs demonstrated negligible apoptosis even at the higher dose.

SACNs Home Preferentially to the Tumors and Bypass Kidney. To elucidate the mechanism underlying the enhanced apoptosis in the tumor and reduced nephrotoxicity evident with the SACNs, we probed the tumor and reticuloendothelial system (RES) organs for the platinum biodistribution. Tumor-bearing animals were dosed with cisplatin or SACNs at doses equivalent to 1 and 3 mg/kg of platinum. As shown in Fig. 4*D*, there was a dose-dependent accumulation of platinum (as quantified per gram of tissue using inductive-coupled plasma atomic absorption spectra) in the RES tissues. Interestingly, the SACNs (3 mg/kg Pt dose) resulted in significantly higher concentration in the tumor than achieved following dosing of an equivalent amount of cisplatin. Furthermore, at this dose, cisplatin resulted in significantly higher platinum build-up in the kidney, which could account for cisplatin-associated nephrotoxicity, compared with the SACN-treated groups.

Efficacy of SACNs in an in Vivo K-Ras$^{LSL/+}$/Pten$^{fl/fl}$ Ovarian Cancer Model. In recent years, it has been well established that frequent somatic PTEN and K-Ras mutations are implicated in wide spectrum of human cancers, including endometrioid ovarian cancer (22–24). As shown in Fig. S6 *A* and *B*, the animals bearing medium and large K-ras$^{LSL/+}$/Pten$^{fl/fl}$ ovarian cancer treated with SACNs (Pt dose equivalent to 3 mg/kg of cisplatin) resulted in greater regression compared with cisplatin treatment. TUNEL revealed apoptosis in both SACN- and cisplatin-treated tumor. However, although cisplatin induced apoptosis of nephrons, negligible cell death was evident in the kidney with SACNs (Fig. S6*C*), which correlated with elevated levels of Pt in the tumor with reduced concentrations in the kidney following SACN treatment compared with cisplatin-treatment (Fig. S6*D*).

Discussion

Supramolecular chemistry, the development of complex chemical systems from molecular building blocks that interact via noncovalent intermolecular forces (25), has emerged as a field that explains and impacts many biological and physical concepts. In an elegant perspective, Jean-Marie Lehn had envisioned a unique paradigm called supramolecular nanochemistry (26). Indeed, gadolinium (III)-encapsulated supramolecular nanoparticles were recently shown to enhance relaxivity with increased sensitivity, and serve as a tool for diagnosis of cancer metastasis (27). In another study, camptothecin was encapsulated in a supramolecular nanoparticle (28). However, although these emerging studies have focused on using supramolecular interactions to encapsulate molecules for targeting cancer, we report here the rational redesign of a cancer chemotherapeutic drug to enable supramolecular assembly into a nanostructure.

Although cisplatin [*cis*-dichlorodiamineplatinum (II)] is the drug of choice as a first or second line chemotherapy for most cancers, its clinical efficacy is dose-limited because of nephrotoxicity, resulting from a peritubular uptake in both proximal and distal tubules mediated by a organic cation transporter 2 (29). As nanoparticles > 5.5 nm can bypass glomerular filtration (13), cisplatin made an excellent candidate for rational engineering into a supramolecular nanostructure to potentially overcome nephrotoxicity. As the first step, we converted *cis*-platinum (II) into an amphiphile via conjugation to a cholesterol succinic acid conjugate, which facilitated the supramolecular assembly of this platinate into SACNs with PC and DSPE-PEG arising from hydrophilic-hydrophobic interactions (30, 31). Cholesterol and PC were selected as both are components of biological cellular membranes, and the 3β-OH group of cholesterol is easily amenable to conjugation, and alter pharmacodynamic/pharmacokinetic profile as well as cellular uptake of the active agent (32). DSPE-PEG was incorporated to impart "stealth" property to SACNs as surface modification of nanoparticles with PEG has been reported to decrease interaction with opsonin (33), and thereby reduce clearance by the RES. Indeed, consistent with the above hypothesis, our biodistribution studies revealed that the SACNs could bypass glomerular filtration in the kidney, evident by the significantly lower Pt concentration in the kidney compared with cisplatin. This finding was further validated by low expression of KIM1, an early marker for kidney injury (34), with

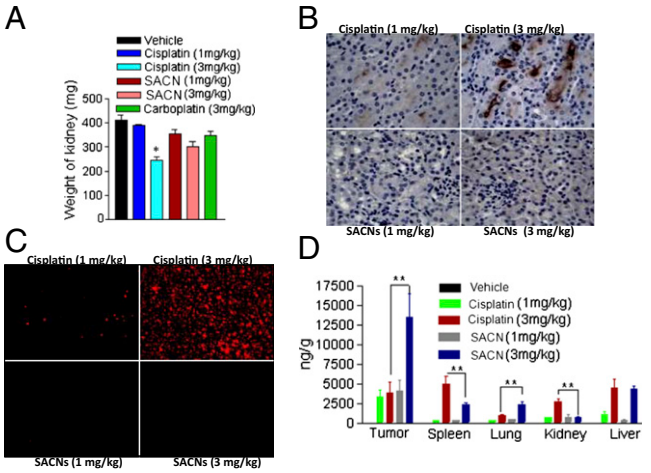

Fig. 4. SACNs preferentially accumulate in the tumor bypassing the kidney, and exert reduced nephrotoxicity. Mice were treated with PBS, carboplatin (3 mg/kg), cisplatin (3 mg/kg and 1 mg/kg), and SACNs (cisplatin NP, 3 mg/kg and 1 mg/kg) ($n = 4$, doses are Pt equivalent) on days 9, 11, and 13 posttumor implantation. (*A*) Bar graph shows weight of excised kidney in different treatment groups. (*B*) Representative images of cross sections of kidney stained for KIM1 expression. Images were captured using a Nikon Eclipse 90i microscope (*Left*). (*C*) Representative images of kidney cross-sections processed for TUNEL as marker apoptosis (*Right*). Images were captured using a Nikon Ti epifluorescence microscope at 20× magnification to capture a large view field; 1,000 × 700 pixels. (*D*) Tissue distribution of platinum in different treatment groups as determined by inductively coupled plasma-MS. $*P < 0.05$, $**P < 0.01$ vs. cisplatin (3 mg/kg)-treated group (ANOVA followed by Newman–Keuls post hoc test).

concomitant decrease in kidney apoptosis observed following SACNs treatment. Furthermore, the SACNs preferentially accumulated in the tumor are consistent with previous reports where such stealth nanosystems were reported to home into the tumors via the EPR effect (5).

Although the SACNs enable enhanced intratumoral concentrations, a critical driver of efficacy is the efficient release of active *cis*-$[Pt(NH_3)_2]^{2+}$ moiety. For example, the stable cyclobutanedicarboxylate chelating ligand lowers the rate of aquation of carboplatin by two-to-four orders of magnitude than cisplatin, and to obtain cytotoxicity comparable to cisplatin a 4- to 20-fold higher dose of carboplatin is required (16). Similarly, AP5280, a N-(2-hydroxypropyl) methacrylamide copolymer-bound platinum was found to exert minimal nephrotoxicity in clinical studies (35), but was less potent than carboplatin because the platinum is held to an aminomalonic acid chelating agent coupled to the COOH terminal glycine of a tetra-peptide spacer (36). The criticality in the amphiphile design in this study was therefore the introduction of the monocarboxylato and O→Pt coordination environment between the platinum and the leaving group, in this case the cholesterol succinic acid conjugate. We have previously demonstrated that this coordination environment was more efficient in releasing activated Pt in a pH-dependent manner than when coordination is via more stable dicarboxylato linkages or monocarboxylato and N→Pt linkage (18, 19). This finding is consistent with the increased potency of SACNs compared with carboplatin as observed in vitro and validated by increased tumor cell apoptosis and necrosis. Interestingly, the SACNs also exhibited slightly improved efficacy compared with cisplatin in the breast cancer (4T1) and LLC cells, and was significantly superior to cisplatin in the hepatocellular carcinoma (7404-CP20), which could be explained by the SACNs harnessing additional mechanisms of uptake into the 7404-CP20 cells besides traditional platinum transporters that are mutated in these cells. Indeed our studies using fluorescently tagged SACNs revealed internalization via endocytosis in a temporal manner. Inhibition of endocytosis decreased the intracellular levels of Pt following SACN treatment to that achieved by treatment with cisplatin. Although previous studies have reported that cholesterol has been shown to facilitate cellular uptake through caveolin-mediated endocytosis (37), we observed that pretreatment of the cells with chlorpromazine, an inhibitor of clathrin-mediated endocytosis, nystatin, a caveolae-mediated endocytosis inhibitor, or cytochalasin D, an inhibitor of macropinocytosis/phagocytosis, could not fully abolish internalization of the SACNs (Fig. S7), which could suggest a redundancy in the mechanisms of SACN internalization. However, it should be noted that recent reports have questioned the specificity of endocytosis inhibitors (38), and in our study we did observe changes in cellular morphology, even at lower doses and short incubation times. Although the SACNs were also internalized in a similar manner by endothelial cells and fibroblasts in vitro (Fig. S7), we anticipate that in vivo the preferential EPR-mediated intratumoral accumulation, and the tendency of SACNs to internalize within the low pH endolysosomal compartment together with the predisposition of the SACNs to release activated *cis*-$[Pt(NH_3)_2]^{2+}$ in an acidic environment, may further contribute to preferential tumor targeting.

Although the SACNs exhibit increased potency, we also observed an increase in the MTD in vivo compared with cisplatin, suggesting that it may be possible to overcome the dosing limits associated with cisplatin in the clinics. We selected the 4T1 breast cancer and the genetically engineered K-ras$^{LSL/+}$/Pten$^{fl/fl}$ ovarian adenocarcinoma mouse models for our in vivo studies because these closely mimic human tumor progression. Interestingly, even at a single sub-MTD platinum dose comparable to the MTD of cisplatin, the SACNs exerted superior antitumor efficacy, both in terms of tumor inhibition and survival, which could be attributed to the preferential accumulation and increased potency. Furthermore, there may be a metronomic dosing effect involved in the therapeutic outcome potentially arising from the sustained release because, even at the lower doses, SACNs were more efficacious than cisplatin. Interestingly, recent clinical reports have indicated that metronomic dosing of cisplatin exerts an antiangiogenic effect (39). Interestingly, we observed that administration of lower multiple doses of cisplatin was more effective in increasing survival compared with a single MTD. This finding indicates that therapeutic efficacy of SACNs can be optimized by tailoring the dosing regimen.

In conclusion, our results support the hypothesis that integrating rational drug design and supramolecular nanochemistry can emerge as a powerful strategy for drug development. Furthermore, because platinum-based chemotherapeutics form the frontline therapy for a broad range of cancers, including testicular, ovarian, cervical, endometrial, bladder, head and neck, lung, and gastro-esophageal cancers, the increased efficacy and improved toxicity profile, resulting from an increase in the molecular dimension through supramolecular assembly, indicates that the constructed nanostructure could translate into the next-generation platinum-based agent in the clinics.

Materials and Methods

Synthesis and Characterization of SACNs. The synthesis and characterization of cholesterol-cisplatin conjugate is described in *SI Materials and Methods*. Briefly, a thin and uniform lipid-drug film of PC, cholesterol-cisplatin conjugate, and DSPE-PEG was coated using a rotary evaporator, then hydrated for 1 h at 60 °C, passed although Sephadex G-25 column, and extruded at 65 °C to obtain sub-200 nm particles. Nanoparticles were analyzed using a nanozetasizer and using cryo-TEM. For release kinetics, drug loaded nanoparticles were suspended in buffer (pH = 5.5 or 7) and sealed in a dialysis membrane (molecular weight cutoff = 500 Da). The dialysis bags were incubated in 30 mL PBS buffer at room temperature with gentle shaking. An aliquot was collected from the incubation medium at predetermined time intervals, and the released drug was quantified.

Cell Viability/Apoptosis Assay. The LLC cells, breast cancer cell line (4T1), and hepatocellular carcinoma cells (CP20) were seeded into 96-well flat bottomed plates (4×10^3 cells per well). Drugs or SACNs were added at equivalent Pt concentrations and incubated for 48 h. Viability was quantified using the

Cell-Titer 96 Aqueous One Solution reagent. Cellular apoptosis was quantified using Annexin-V-Alexa Fluor 488 conjugate and propidium iodide staining followed by FACS.

SACN Internalization Study. The 4T1 cells were seeded on glass cover-slips and treated with FITC-encapsulated SACNs for a time-course ranging from 30 min to 18 h. At the indicated times, cells were washed twice in PBS and incubated in LysoTracker red for 30 min at 37 °C. Images taken in three random fields were captured at using an inverted epifluorescence deconvolution microscope (Nikon). To study the role of endocytosis in SACN internalization, the cells were incubated at 4 °C or pretreated with endocytosis inhibitors (described in detail in *SI Materials and Methods*).

In Vivo Murine 4T1 Breast Cancer Model. The 4T1 breast cancer cells (3×10^5) were implanted subcutaneously in the flanks of 4-wk-old BALB/c mice. The drug therapy consisted of intravenous administration of SACNs (1 mg/kg and 3 mg/kg equivalent Pt dose), cisplatin (1 mg/kg and 3 mg/kg equivalent Pt dose), and carboplatin (3 mg/kg equivalent Pt dose). PBS (100 μL) by tail-vain injection was used as a control for drug treatment. Treatment was started on day 9 postimplantation, and administered every alternate day till day 13. The tumor volumes and body weights were monitored on a daily basis. The tumor volume was calculated by using the formula, $L \times B^2$. All animal procedures were approved by the Harvard Institutional Use and Care of Animals Committee.

Transgenic Ovarian Cancer Tumor Model. Ovarian adenocarcinomas were induced in genetically engineered K-ras$^{LSL/+}$/Pten$^{fl/fl}$ mice via intrabursal delivery of adenovirus carrying Cre recombinase. Tumor cells were engineered to express luciferase once activated by Adeno-Cre, to make tumor imaging feasible before and after drug treatment. The drug therapy consisted of tail vein administration of SACNs (3 mg/kg equivalent Pt dose), cisplatin (3 mg/kg equivalent Pt dose), or PBS (100 μL). Each animal was dosed three times over the course of treatment given every alternate day. Treatment efficacy was quantified by examining the fold increase in bioluminescence of the post-treatment signal compared with baseline. A detailed description is available in *SI Materials and Methods*.

Biodistribution of SACNs. Tumor-bearing animals were treated as described earlier. Organs were harvested, weighed, and dissolved in concentrated HNO_3. To these mixtures 30% (vol/vol) H_2O_2 was added; the resulting solutions were stirred for 24 h at room temperature and then heated for another 12 h to evaporate the liquids. All solid residues were redissolved in 1 mL water and then amount of platinum was measured by inductive-coupled plasma-atomic absorption spectrometry/MS.

Histopathology. The tissues were fixed in 10% formalin, paraffin-embedded, and sectioned at the Harvard Medical School Core Facility. Tumor and kidney paraffin sections were deparaffinized and stained with a standard TMR red fluorescent TUNEL kit following the manufacturer's protocol (In Situ Cell Death Detection Kit, TMR-Red; Roche). The kidney sections were also immunolabeled for KIM1 expression. Images were obtained using a Nikon Eclipse TE2000 fluorescence microscope equipped with red filter. For further details see *SI Materials and Methods*.

ACKNOWLEDGMENTS. This work is supported by US Department of Defense Breast Cancer Research Program Era of Hope Scholar Award W81XWH-07-1-0482; a Department of Defense Collaborative Innovator Grant; National Institutes of Health Grant R01 CA135242-01A2; a Charles A. King Trust Fellowship; a Department of Defense Breast Cancer Research Program Postdoctoral Fellowship Award; the Burroughs-Wellcome Foundation; a Harvard Ovarian Cancer Spore Award; the Canary Fund; the Mary Kay Ash Foundation; and a V Foundation for Cancer Research Scholar Award.

1. Jemal A, Center MM, DeSantis C, Ward EM (2010) Global patterns of cancer incidence and mortality rates and trends. *Cancer Epidemiol Biomarkers Prev* 19:1893–1907.
2. World Health Organization (2008) WHO Cancer Report. Available at http://www.who.int/cancer/en/. Accessed June 12, 2012.
3. Ferrari M (2005) Cancer nanotechnology: Opportunities and challenges. *Nat Rev Cancer* 5:161–171.
4. Yuan F, et al. (1994) Microvascular permeability and interstitial penetration of sterically stabilized (stealth) liposomes in a human tumor xenograft. *Cancer Res* 54:3352–3356.
5. Northfelt DW, et al. (1996) Doxorubicin encapsulated in liposomes containing surface-bound polyethylene glycol: Pharmacokinetics, tumor localization, and safety in patients with AIDS-related Kaposi's sarcoma. *J Clin Pharmacol* 36:55–63.
6. Desai N, et al. (2006) Increased antitumor activity, intratumor paclitaxel concentrations, and endothelial cell transport of cremophor-free, albumin-bound paclitaxel, ABI-007, compared with cremophor-based paclitaxel. *Clin Cancer Res* 12:1317–1324.
7. Zamboni WC (2008) Concept and clinical evaluation of carrier-mediated anticancer agents. *Oncologist* 13:248–260.
8. Kelland L (2007) The resurgence of platinum-based cancer chemotherapy. *Nat Rev Cancer* 7:573–584.
9. Avgoustakis K, et al. (2002) PLGA-mPEG nanoparticles of cisplatin: In vitro nanoparticle degradation, in vitro drug release and in vivo drug residence in blood properties. *J Control Release* 79:123–135.
10. Haxton KJ, Burt HM (2009) Polymeric drug delivery of platinum-based anticancer agents. *J Pharm Sci* 98:2299–2316.
11. Zamboni WC, et al. (2004) Systemic and tumor disposition of platinum after administration of cisplatin or STEALTH liposomal-cisplatin formulations (SPI-077 and SPI-077 B103) in a preclinical tumor model of melanoma. *Cancer Chemother Pharmacol* 53:329–336.
12. White SC, et al. (2006) Phase II study of SPI-77 (sterically stabilised liposomal cisplatin) in advanced non-small-cell lung cancer. *Br J Cancer* 95:822–828.
13. Choi HS, et al. (2007) Renal clearance of quantum dots. *Nat Biotechnol* 25:1165–1170.
14. Madias NE, Harrington JT (1978) Platinum nephrotoxicity. *Am J Med* 65:307–314.
15. Davies MS, Berners-Price SJ, Hambley TW (2000) Slowing of cisplatin aquation in the presence of DNA but not in the presence of phosphate: improved understanding of sequence selectivity and the roles of monoaquated and diaquated species in the binding of cisplatin to DNA. *Inorg Chem* 39:5603–5613.
16. Knox RJ, Friedlos F, Lydall DA, Roberts JJ (1986) Mechanism of cytotoxicity of anticancer platinum drugs: Evidence that cis-diamminedichloroplatinum(II) and cis-diammine-(1,1-cyclobutanedicarboxylato)platinum(II) differ only in the kinetics of their interaction with DNA. *Cancer Res* 46:1972–1979.
17. Los G, et al. (1991) Cellular pharmacokinetics of carboplatin and cisplatin in relation to their cytotoxic action. *Biochem Pharmacol* 42:357–363.
18. Paraskar A, et al. (2011) Rationally engineered polymeric cisplatin nanoparticles for improved antitumor efficacy. *Nanotechnology* 22:265101.
19. Paraskar AS, et al. (2010) Harnessing structure-activity relationship to engineer a cisplatin nanoparticle for enhanced antitumor efficacy. *Proc Natl Acad Sci USA* 107:12435–12440.
20. Sengupta S, et al. (2005) Temporal targeting of tumour cells and neovasculature with a nanoscale delivery system. *Nature* 436:568–572.
21. Shen DW, Akiyama S, Schoenlein P, Pastan I, Gottesman MM (1995) Characterisation of high-level cisplatin-resistant cell lines established from a human hepatoma cell line and human KB adenocarcinoma cells: Cross-resistance and protein changes. *Br J Cancer* 71:676–683.
22. Sato N, et al. (2000) Loss of heterozygosity on 10q23.3 and mutation of the tumor suppressor gene PTEN in benign endometrial cyst of the ovary: possible sequence progression from benign endometrial cyst to endometrioid carcinoma and clear cell carcinoma of the ovary. *Cancer Res* 60:7052–7056.
23. Cuatrecasas M, et al. (1998) K-ras mutations in nonmucinous ovarian epithelial tumors: a molecular analysis and clinicopathologic study of 144 patients. *Cancer* 82:1088–1095.
24. Dinulescu DM, et al. (2005) Role of K-ras and Pten in the development of mouse models of endometriosis and endometrioid ovarian cancer. *Nat Med* 11:63–70.
25. Lehn JM (1995) *Supramolecular Chemistry: Concepts and Perspectives* (VCH, New York).
26. Lehn JM (2002) Toward complex matter: Supramolecular chemistry and self-organization. *Proc Natl Acad Sci USA* 99:4763–4768.
27. Chen KJ, et al. (2011) A small MRI contrast agent library of gadolinium(III)-encapsulated supramolecular nanoparticles for improved relaxivity and sensitivity. *Biomaterials* 32:2160–2165.
28. Chen KJ, et al. (2012) The therapeutic efficacy of camptothecin-encapsulated supramolecular nanoparticles. *Biomaterials* 33:1162–1169.
29. Yao X, Panichpisal K, Kurtzman N, Nugent K (2007) Cisplatin nephrotoxicity: A review. *Am J Med Sci* 334:115–124.
30. Bedu-Addo FK, Tang P, Xu Y, Huang L (1996) Interaction of polyethyleneglycol-phospholipid conjugates with cholesterol-phosphatidylcholine mixtures: Sterically stabilized liposome formulations. *Pharm Res* 13:718–724.
31. Matsumori N, et al. (2004) An amphotericin B-ergosterol covalent conjugate with powerful membrane permeabilizing activity. *Chem Biol* 11:673–679.
32. Torchilin VP (2005) Recent advances with liposomes as pharmaceutical carriers. *Nat Rev Drug Discov* 4:145–160.
33. Mosqueira VC, et al. (2001) Relationship between complement activation, cellular uptake and surface physicochemical aspects of novel PEG-modified nanocapsules. *Biomaterials* 22:2967–2979.
34. Vaidya VS, et al. (2010) Kidney injury molecule-1 outperforms traditional biomarkers of kidney injury in preclinical biomarker qualification studies. *Nat Biotechnol* 28:478–485.
35. Rademaker-Lakhai JM, et al. (2004) A Phase I and pharmacological study of the platinum polymer AP5280 given as an intravenous infusion once every 3 weeks in patients with solid tumors. *Clin Cancer Res* 10:3386–3395.
36. Lin X, et al. (2004) Improved targeting of platinum chemotherapeutics. the antitumour activity of the HPMA copolymer platinum agent AP5280 in murine tumour models. *Eur J Cancer* 40:291–297.
37. Sugano K, et al. (2010) Coexistence of passive and carrier-mediated processes in drug transport. *Nat Rev Drug Discov* 9:597–614.
38. Vercauteren D, et al. (2010) The use of inhibitors to study endocytic pathways of gene carriers: Optimization and pitfalls. *Mol Ther* 18:561–569.
39. Jian W, Levitt JM, Lerner SP, Sonpavde G (2009) Preclinical antitumor and anti-angiogenic activity of a metronomic schedule of cisplatin against human transitional cell carcinoma (TCC). *J Clin Oncol* 27:e16018.